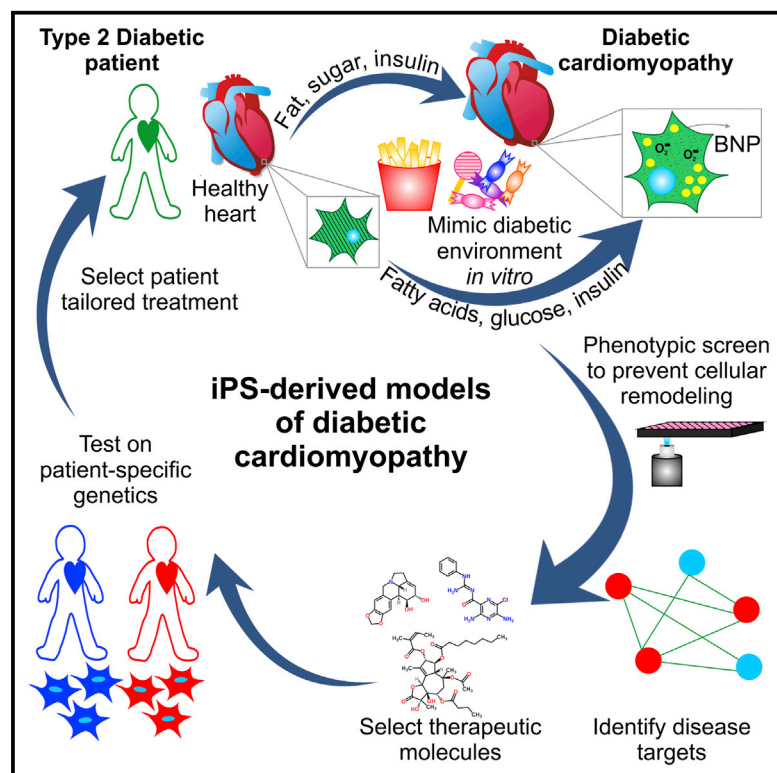# Disease Modeling and Phenotypic Drug Screening for Diabetic Cardiomyopathy using Human Induced Pluripotent Stem Cells

Graphical Abstract

Authors

Faye M. Drawnel, Stefano Boccardo, ..., Jacques Bailly, Roberto Iacone

Correspondence

roberto.iacone@roche.com

In Brief

Diabetes causes pathological remodeling of cardiac muscle, which impairs heart function. Drawnel et al. use induced-pluripotent-stem-cell-derived cardio-myocytes to develop environmental and patient-specific in vitro models recapitulating the condition. These models are harnessed in a phenotypic screening assay that identifies candidate protective molecules.

Highlights

Diabetic cardiomyopathy can be induced in vitro by environmental or genetic means

Diabetic patient-specific cardiomyocytes show baseline cardiomyopathy

The extent of patient-specific cardiomyopathy is clinically correlated

Phenotypic screening identifies drugs that rescue the disease phenotype

Accession Numbers

GSE62203

CrossMark

CellPress

Disease Modeling and Phenotypic Drug Screening for Diabetic Cardiomyopathy using Human Induced Pluripotent Stem Cells

Faye M. Drawnel,[1] Stefano Boccardo,[1,2] Michael Prummer,[1] Frédéric Delobel,[1] Alexandra Graff,[3] Michael Weber,[1] Régine Gérard,[1] Laura Badi,[1] Tony Kam-Thong,[1] Lei Bu,[4] Xin Jiang,[4] Jean-Christophe Hoflack,[1] Anna Kiialainen,[1] Elena Jeworutzki,[1] Natsuyo Aoyama,[5] Coby Carlson,[5] Mark Burcin,[1] Gianni Gromo,[1] Markus Boehringer,[1] Henning Stahlberg,[3] Benjamin J. Hall,[1] Maria Chiara Magnone,[1] Kyle Kolaja,[5] Kenneth R. Chien,[6,7] Jacques Bailly,[1] and Roberto Iacone[1,*]

[1]Roche Pharma Research & Early Development, Roche Innovation Center Basel, 4070 Basel, Switzerland
[2]Department of Chemistry and Chemical Biology, Harvard University, Cambridge, MA 02138, USA
[3]Center for Cell Imaging and Nano Analytics, Biozentrum, Department for Biosystems Science and Engineering, University of Basel, 4058 Basel, Switzerland
[4]The Cardiovascular Research Center, Richard B. Simches Research Center, Massachusetts General Hospital, Suite 3201, Boston, MA 02114, USA
[5]Cellular Dynamics International, Madison, WI 53711, USA
[6]Departments of Cell and Molecular Biology and of Medicine Huddinge, Karolinska Institutet, 171 77 Stockholm, Sweden
[7]Harvard Department of Stem Cell and Regenerative Biology, Harvard University, Cambridge, MA 02138, USA
*Correspondence: roberto.iacone@roche.com
http://dx.doi.org/10.1016/j.celrep.2014.09.055

SUMMARY

Diabetic cardiomyopathy is a complication of type 2 diabetes, with known contributions of lifestyle and genetics. We develop environmentally and genetically driven in vitro models of the condition using human-induced-pluripotent-stem-cell-derived cardiomyocytes. First, we mimic diabetic clinical chemistry to induce a phenotypic surrogate of diabetic cardiomyopathy, observing structural and functional disarray. Next, we consider genetic effects by deriving cardiomyocytes from two diabetic patients with variable disease progression. The cardiomyopathic phenotype is recapitulated in the patient-specific cells basally, with a severity dependent on their original clinical status. These models are incorporated into successive levels of a screening platform, identifying drugs that preserve cardiomyocyte phenotype in vitro during diabetic stress. In this work, we present a patient-specific induced pluripotent stem cell (iPSC) model of a complex metabolic condition, showing the power of this technique for discovery and testing of therapeutic strategies for a disease with ever-increasing clinical significance.

INTRODUCTION

The World Health Organization estimates that the lethal clinical trajectory of type 2 diabetes mellitus (T2DM) will make it the sev-enth leading cause of death worldwide by 2030. Cardiovascular disease is the primary cause of death in this group, with data indicating that diabetes has a negative effect on cardiac muscle, independent of concurrent vascular influences such as coronary artery disease (Devereux et al., 2000). This condition is known as diabetic cardiomyopathy (DCM), which progresses to dilated cardiomyopathy and heart failure (Mandavia et al., 2013). T2DM induces specific cellular and molecular changes in the cardiomyocyte (CM), which lead to the pathology of these conditions. For example, the majority of the ATP required by healthy adult CMs is produced by fatty acid β-oxidation, with only a minor contribution from glucose and lactate oxidation. During nondiabetic cardiac disease and injury, CM metabolism reverts to an immature, fetal profile, with increased reliance on glucose oxidation (Lopaschuk and Jaswal, 2010). However, as a result of myocardial insulin resistance, T2DM promotes fatty acid β-oxidation in CMs, with pathological consequences (Heather and Clarke, 2011). First, fatty acid β-oxidation produces less ATP per O_2 consumed, reducing myocardial efficiency (Lorenzo et al., 2013). Second, toxic lipid metabolites such as ceramide accumulate in the CM, a response that is exacerbated by hyperlipidemia. Lastly, these metabolic changes distort CM structure. Mitochondrial dysfunction and reactive oxygen species (ROS) production activate ROS-sensitive proteases, which cleave myofilament proteins (Steinberg, 2013). Concurrently, oxidation-dependent ER stress impairs protein maturation and promotes degradation of newly synthesized proteins at the ER (Minamino and Kitakaze, 2010). Proteolytic damage and inadequate protein production synergize, resulting in loss of sarcomeric integrity. Together, these changes result in the clinical symptoms of DCM.

Despite its profound clinical impact, there is no specific treatment for DCM, and the complex etiology of the condition

makes drug screening problematic. Here, we aimed to develop in vitro DCM models using human induced pluripotent stem cell (iPSC)-derived CMs. These cells have been used in studies of cardiac hypertrophy, arrhythmia, toxicology, and metabolism (Carlson et al., 2013; Ma et al., 2011). Apart from the advantages of using cells of human origin, harnessing iPSC technology enables the generation of patient-specific models of disease. We show that a surrogate DCM phenotype emerges in these cells upon exposure to a prodiabetic environment and that a similar phenotype is present in the absence of a diabetic stimulus in two diabetic-patient-specific cell lines. We utilize both of these models to establish a screening platform for the identification of small molecules that rescue CM function in vitro during diabetic stress.

RESULTS

Metabolic Manipulation Alters Maturation Status of iPSC-CMs

Before investigating diabetes-dependent changes in CM functionality, we considered how to best use iPSC-CMs in our study. DCM is a disease of adult CMs, which have defined structural, molecular, and metabolic characteristics. Human iPSC-CMs more closely resemble neonatal CMs, with a degree of flexibility that can change cellular phenotype, depending on the experimental conditions (Carlson et al., 2013). We hypothesized that promoting adult patterns of metabolic activity would give a more-suitable baseline on which to model the response of CMs to diabetic conditions. To test the effect of controlling cellular metabolism, CMs were exposed to either standard manufacturer's maintenance medium (SM) or maturation medium (containing insulin and fatty acids, but no glucose) for 3 days after plating. In maturation medium (MM), ATP synthesis must be maintained by fatty acid β-oxidation, mimicking the metabolic substrate usage of the adult ventricular CM. As changes to cellular metabolism have been associated with promotion of cellular maturity (Carlson et al., 2013), we determined the structural, molecular, and electrophysiological impact of this manipulation. First, we quantified the striated pattern of immunofluorescent (IF) α-actinin staining (CM score) as a correlate of the development of CM subcellular structure and sarcomeric integrity. Culturing iPSC-CMS in MM for 3 days increased CM score (Figures 1A and 1B), relative to cells grown in SM. Sarcomere length also increased (Figure 1C). These changes in subcellular structure were accompanied by altered electrophysiological properties (Figure 1D). The upstroke velocity and duration of the action potential were increased in cells grown in MM (Figures 1E and 1F), characteristics associated with CM maturation (Yang et al., 2014). The total and live cell count did not change over the 3-day culture period (Figures 1G and 1H), and there was no increase in the proportion of dead cells (Figure 1I), excluding the possibility that MM selects against an immature cell population. Next, we analyzed gene expression patterns before and after the 3-day period in MM (Figure 1J). Genes annotated by the striated muscle contraction gene ontology term were enriched over time (Figure 1J), including myosin light chains: *MYL2*; *MYL3*; and *MYL4*. Genes involved in regulation of sarcoplasmic retic-

ulum (SR) calcium content (*SERCA2A* and *PLN*) were also increased, whereas expression of fetally enriched genes (*NPPA*, *NPPB*, and *ACTA1*) was repressed. Together, these results suggest that MM shifts the gene-expression profile of iPSC-CMs toward an adult-like pattern (Yang et al., 2014). Interestingly, expression of voltage-gated sodium channel subunits *SCN5a* (pore-forming subunit) and *SCN2B* (regulatory subunit) also increased upon culture in MM (Figure 1K). To test whether this was associated with a change in the properties of the CM sodium current, we performed patch clamp experiments. Consistent with a 2-fold increase in expression of the *SCN5a* subunit (Figure 1K), there was a strong statistical trend toward doubling of peak sodium current, measured by whole-cell voltage clamp and normalized to cell capacitance (Figure 1L; p = 0.055) following 3 days culture in MM. Additionally, we observed an increase in the slope of the sodium channel activation curve between −60 and −30 mV, consistent with an increase in cellular excitability over this maturation period (Figure 1M). Together, these data suggest that culture in MM induces expression and sarcolemmal integration of functional voltage-gated sodium channels. As these channels generate the rapid depolarization phase of the CM action potential, these data are in agreement with the increased action potential upstroke velocity shown in Figure 1F.

Taken as a whole, these data show structural, molecular, and electrophysiological characteristics associated with maturing CMs became more pronounced following incubation in MM. Although the cells do not attain a full adult phenotype, metabolic dependence on fatty acid β-oxidation recapitulates cellular activities prominent in more mature cells, giving a more-appropriate baseline for DCM modeling.

Exposure to a Diabetogenic Environment Induces a Phenotypic Surrogate of Diabetic Cardiomyopathy

Clinically, diabetic patients show hyperglycemia, hyperlipidemia, and altered plasma levels of neurohormonal and inflammatory mediators (Mandavia et al., 2013). We hypothesized that exposure of human-iPSC-derived CMs to a diabetic-like environment would promote cell-autonomous features similar to DCM. During the 3-day period in MM, CMs are exposed to persistent insulin signaling in the absence of glucose, forcing adaptation to fatty acids as a carbon source. We hypothesized that reintroduction of glucose following cellular maturation in MM (Figure S1A) would mimic the conditions found in diabetes: glucose excess despite a metabolic reliance on fatty acids. To quantify the cellular response, brain natriuretic peptide (BNP) release was measured. Addition of glucose dose-dependently increased BNP secretion over a 2 day culture period (Figure 2A). As T2DM is diagnosed when fasting plasma glucose concentration exceeds 7 mM and 10 mM glucose-induced maximal BNP release, this concentration was used for the continuation of our study. Next, we tested whether addition of known hormonal mediators of diabetes, endothelin 1 (ET-1) and cortisol, enhanced BNP production. Maximal BNP secretion was consistently produced by culture of CMs in a diabetic milieu (DM) of glucose (10 mM), ET-1 (10 nM), and cortisol (1 μM) together (Figure 2B). Microarray analysis confirmed reversion of DM-treated CMs
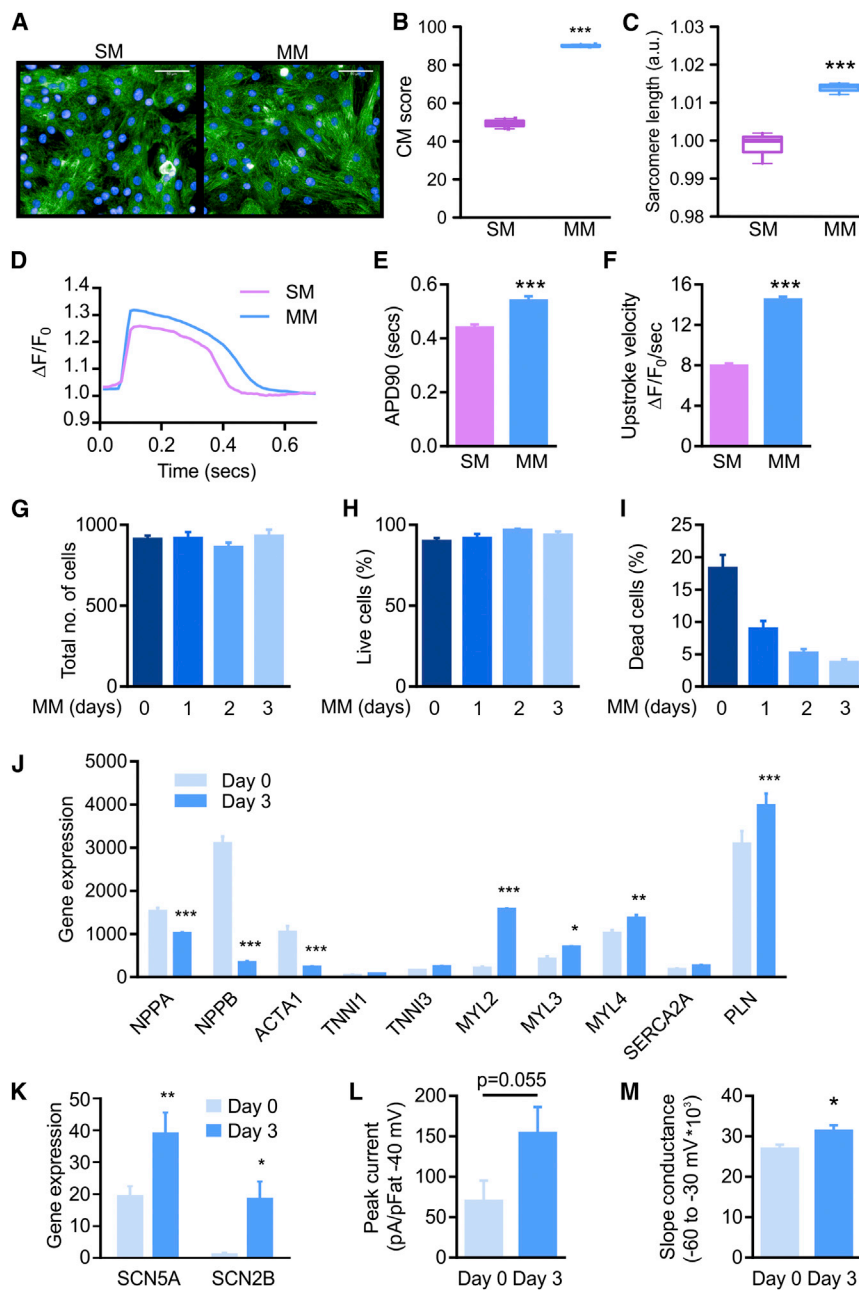
Figure 1. Metabolic Manipulation of iPSC-CMs Enhances Characteristics Associated with Maturing CMs

(A) Representative image of SM/MM-treated cells. α-actinin (green); DAPI (blue); scale bar, 50 μm.

(B) CM score following exposure to standard medium (SM) or maturation medium (MM) for 3 days.

(C) Sarcomere length in CM exposed to SM or MM for 3 days. a.u., arbitrary units.

(D) Representative spontaneous action potential in CMs exposed to SM or MM for 3 days. CMs were loaded with a voltage-sensitive dye and change in fluorescence intensity monitored over time.

(E) Action potential duration at 90% repolarization (APD90) calculated from traces of voltage-sensitive dye fluorescence intensity in CMs exposed to SM or MM for 3 days.

(F) Action potential upstroke velocity calculated from traces as in (A) of CMs treated with SM or MM for 3 days.

(G) Total number of CMs after 0, 1, 2, or 3 days culture in MM.

(H) Percent of live cells measured by calcein-AM uptake in CMs exposed to 0, 1, 2, or 3 days of culture in MM.

(I) Percent of dead cells measured by ethidium-homodimer-1 uptake in CMs exposed to 0, 1, 2, or 3 days of culture in MM. The higher percent of dead cells at day 0 reflects nonadherent cells remaining after plating.

(J) mRNA expression of *TMOD1*, *TNNI1*, *TNNI3*, *MYL2*, *MYL3*, *MYL4*, and *MYBPC3* measured by microarray in cells before (day 0) and after (day 3) maturation in MM.

(K) mRNA expression of *SCN5a* and *SCN5b* measured by microarray in cells before (day 0) and after (day 3) maturation in MM.

(L) Peak whole-cell sodium current measured at −40 mV and normalized to cell capacitance to control for cell size in day 0 and day 3 CMs.

(M) Slope of the sodium channel activation curve measured between −60 and −30 mV in day 0 and day 3 CMs.

Data represent the mean ± SEM of at least three experiments. *$p < 0.05$, **$p < 0.01$, and ***$p < 0.001$.

to a pattern of gene expression associated with hypertrophic stress (Taegtmeyer et al., 2010). The hypertrophic markers *NPPA*, *NPPB*, *ACTA1*, and *MYH7* were elevated at the mRNA level (Figure S1B) whereas *MYH6* was diminished. mRNA levels of the chamber-specific markers *MYL7* (atrial), *MYL2* (ventricular), and *IRX4* (ventricular) were unchanged (Figure S1B), verifying that the extent and nature of cellular differentiation was not altered by DM treatment. Confirming the prohypertrophic and pathological effect of the diabetic milieu, CMs treated with DM released greater amounts of the cardiac pathological stress proteins troponin I and FABP3 (Figures S1C and S1D).

When DM-treated CMs were examined by IF, we observed increases in cellular (Figures 2C and 2E) and nuclear surface area (Figures 2C and S1E), definitive confirmation of hypertrophy. Interestingly, a loss of sarcomeric integrity was also apparent. The regular striped pattern of α-actinin staining became diffuse (Figure 2C). Consequently, CM score was diminished after 2 days exposure to DM (Figure 2D). Next, we tested whether the response to DM persisted beyond the duration of the stimulus. After 48 hr exposure to DM, DM was replaced with MM for a further 48 hr and CM score, nuclear area, and BNP release quantified at both 48 and 96 hr posttreatment. Removal of DM did not permit CM score (Figure S1F) or nuclear area (Figure S1G) to return to the level of the untreated control. Indeed, values for CM score and nuclear area after stimulus washout were similar to those measured
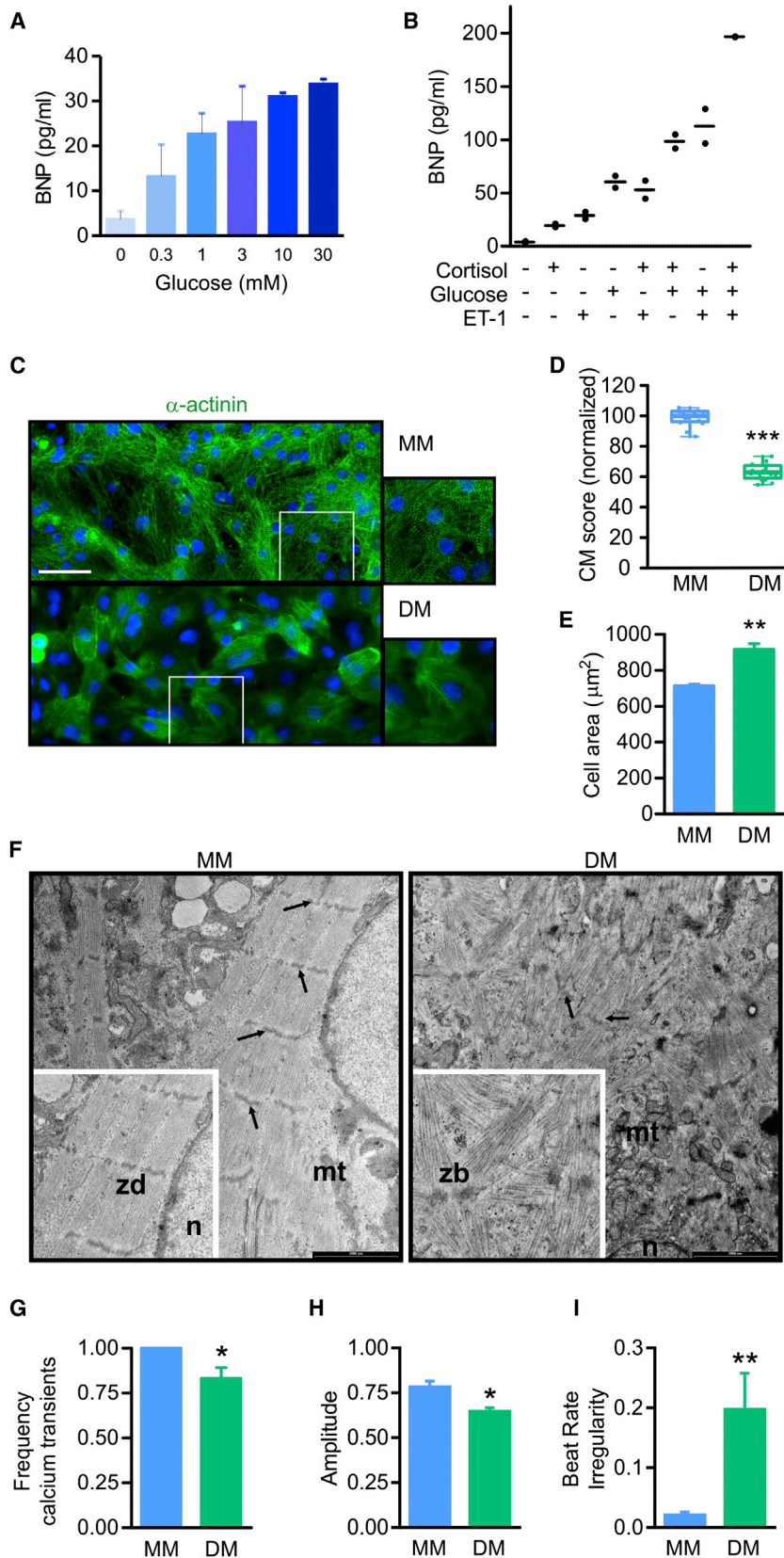
Figure 2. A Diabetogenic Extracellular Environment Induces CM Hypertrophy and Loss of Sarcomeric Integrity

(A) Dose response for glucose-stimulated BNP secretion. BNP in the culture supernatant was quantified after 2 days treatment of CMs with 0.3–30 mM glucose in MM.

(B) BNP secretion after 2 days treatment of CMs with MM plus glucose (10 mM), ET-1 (10 nM), and cortisol (1 μM) singly or in combination.

(C) IF images of CMs grown in MM or diabetic medium (DM: 10 mM glucose, 10 nM ET-1, and 1 μM cortisol) for 2 days. α-actinin (green); DAPI (blue); scale bar, 50 μm. Top panels: MM-treated cells. Bottom panels: DM-treated cells. The area within the white square is shown at a higher magnification on the right; scale bar, 20 μm.

(D) Quantification of CM score in CMs exposed to MM or DM for 2 days as in (C).

(E) Cell surface area of CMs treated as in (C).

(F) Transmission electron micrographs of CMs cultured in MM or DM for 2 days (scale bar, 2 μm). Black arrows identify z discs; mt, mitochondria; n, nucleus; z, z body; zd, z disc.

(G) Calcium transient frequency in CMs exposed to MM or DM. CMs were loaded with calcium 5 and fluorescence intensity monitored over 30 s.

(H) CM beat amplitude in cells as in (C) measured by impedance monitoring.

(I) Beat-rate irregularity in CMs as in (C). Cellular impedance was monitored and the interval between CM beats measured. Beat-rate irregularity, the coefficient of variation of the beat interval.

Data represent the mean ± SEM of at least three experiments. *$p < 0.05$, **$p < 0.01$, and ***$p < 0.001$. See also Figures S1 and S2.

with our standard 48 hr DM treatment (Figures S1F and S1G). Conversely, BNP release fell to negligible levels following DM removal (Figure S1H), similar to that of untreated control CMs. To confirm that the structural changes we observed by IF were truly a reflection of sarcomeric disorder, we examined CMs at the ultrastructural level (Figure 2F). Transmission electron microscopy of CMs cultured in MM for 48 hr confirmed a regular parallel arrangement of myofilaments within sarcomeres and prominent z discs. Although isolated areas of well-organized CM structure were identifiable in DM-treated CMs, the majority of cells exhibited myofilament disarray and a lack of pronounced z discs. Instead, we observed the emergence of punctate electron dense structures known as z bodies, which appear when the linear structure of the z disc is absent. These features are similar to those observed in failing human heart specimens and genetic cardiomyopathies (Sun et al., 2012), confirming that the changes in the pattern of sarcomere staining do reflect structural abnormality.

As loss of sarcomeric integrity disturbs the close physical coupling between calcium release units and contractile proteins (Bers, 2008), we investigated the functional consequences of sarcomeric disarray. In CMs exposed to DM, the frequency of systolic calcium transients decreased (Figure 2G). Furthermore, impedance-based monitoring (Abassi et al., 2012) revealed that the amplitude of CM beats was reduced in DM-treated cells (Figure 2H). Beat rate irregularity, a measure of the variability of the interval between beats, was increased (Figure 2I). These data show a functional impact of DM treatment, with fewer calcium transients producing poorly coordinated, weaker, and irregular CM beats.

In Vitro Induction of DCM Promotes Lipid Accumulation and Peroxidation

Diabetic CMs display a number of additional specific features that contribute to the pathogenesis of structural disarray, such as lipid accumulation and oxidative stress. To test whether these processes were active in our system, we estimated intracellular lipid accumulation. Following 2 days exposure to DM, lipid accumulated in the cytosol (Figures S2A and S2B). Quantification of peroxidation levels revealed that the deposited lipid was extensively oxidized (Figures S2C and S2D), indicating that, under DM-treated conditions, CMs are exposed to oxidative stress. To gain a holistic view of the molecular changes that may drive the observed phenotypes, we analyzed gene-expression profiles in DM-treated CMs and interpreted the data using gene set enrichment analysis (GSEA). Sixty-four gene sets were positively enriched in the diabetic condition, whereas 140 gene sets displayed diminished expression (Table S1). We generated an enrichment map of the GSEA, clustering and categorizing significantly altered gene sets (Figure S2E). We identified positive enrichment of major clusters related to cellular metabolism: genes involved in the tricarboxylic acid (TCA) cycle (e.g., pyruvate dehydrogenase kinase), mitochondrial electron transport chain (e.g., ATP synthase subunits and cytochrome C), and glucose metabolism (e.g., enolase) were upregulated. Other enriched categories included cell adhesion (e.g., integrins) and extracellular matrix deposition (e.g., collagens). The expression of several gene clusters was diminished after DM exposure,

including genes involved in the cell cycle (e.g., DNA replication proteins), protein translation (e.g., ribosomal proteins and eukaryotic initiation factors), and the unfolded protein/ER stress response (e.g., ATF4 and CHOP10). Altogether, in the DM condition, there is a generalized increase in metabolic gene expression and suppression of genes controlling protein synthesis and the cellular response to dysfunctional protein production. Despite an excess of metabolic intermediates and activated metabolic pathways, the ability of the cell to produce new proteins appears to be compromised.

The results presented suggest that CMs exposed to a diabetic milieu of glucose, ET-1, and cortisol recapitulate a diabetic cardiomyopathic phenotype in vitro. DM-treated cells show disorganized sarcomeres, altered calcium transients, cellular hypertrophy, lipid intracellular accumulation, oxidative stress, and deficits in the expression of genes controlling protein production. The presence of multiple facets of the DCM cellular phenotype in our model suggests that the changes we observe are not simply a result of cellular dedifferentiation but transition to a disease-like state.

CMs Derived from Diabetic-Patient-Specific iPSCs Show a Cardiomyopathic Phenotype in the Absence of a Diabetic Stimulus

We next wished to examine whether the in vitro phenotype of our model is similar to that of diabetic patients. Considering the difficulty of obtaining adult human cardiac material, we tested whether iPSC technology could be harnessed to create diabetic-patient-specific CM models. Using iPSC-CMs derived from different patients, we could study the variable penetrance of preexisting genetic and/or retained epigenetic factors on CM phenotype. We categorized diabetic patients with different clinical histories using stringent inclusion and exclusion criteria. To best test the likelihood that genetic/epigenetic predisposition would affect phenotype, two diabetic extreme phenotypes were selected: fast progression (FP), with development of cardiovascular disease (CVD) within 5 years of initial diabetes diagnosis, and slow progression (SP), with no CVD despite 15 years T2DM (Table S2). Dermal fibroblasts from these patients were retrovirally reprogrammed to pluripotency with OCT4, SOX2, KLF4, and c-MYC. The iPSCs generated were karyotypically normal (Figure S3A) and could be induced to differentiate into embryoid bodies that express markers of the three germ layers (Table S3). FP and SP CMs were derived from iPSCs using identical standard cardiogenic methods (Ma et al., 2011). Both FP and SP cultures were spontaneously contractile, with greater than 90% of the cells cTnT positive. Next, we characterized CMs as above. When cultured in MM (+insulin, +fatty acids, and −glucose) in the absence of diabetic stress, CM score was lower in SP and FP CMs than standard CMs, indicating sarcomeric disarray (Figures 3B and 3C). Furthermore, the frequency of calcium transients was reduced in the FP cells (Figure 3D) whereas beat rate irregularity was increased (Figure 3E). FP CMs also accumulated more intracellular peroxidized lipid (Figures 3F, 3G, and S3B), indicative of oxidative stress. These findings are similar to those observed in standard CMs on exposure to DM. Interestingly, in the absence of the diabetic milieu, SP CMs had an intermediate
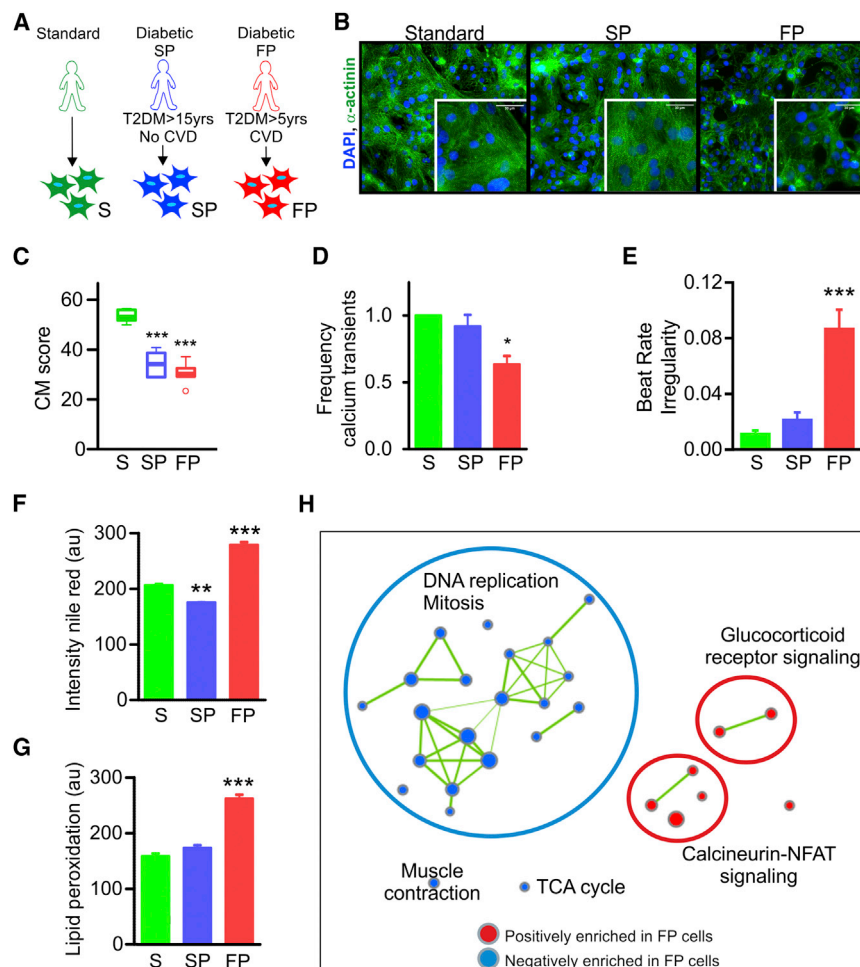
Figure 3. Diabetic-Patient-Specific CMs Exhibit a Diabeto-Mimetic Phenotype in the Absence of Cellular Stimulation

(A) Cartoon to show the three types of CM. CM were derived from standard iPSC (S, green), slow-progressing diabetic iPSC (SP, blue), and fast-progressing diabetic iPSC (FP, red).

(B) IF images of standard, SP, and FP CMs. α-actinin (green) and DAPI (blue); scale bar, 30 μm.

(C) CM score of standard, SP, and FP CMs cultured in MM for 2 days.

(D) Calcium-transient frequency in standard, SP, and FP CMs exposed to MM for 2 days.

(E) Beat-rate irregularity in S, SP, and FP CMs.

(F) Quantification of lipid accumulation by nile red staining in standard, SP, and FP CMs cultured in MM for 2 days.

(G) Quantification of lipid peroxidation in standard, SP, and FP CMs cultured in MM for 2 days.

(H) Enrichment map to represent gene sets enriched following mRNA sequencing of FP and SP CMs to compare gene expression between the two cell types. mRNA sequencing was performed on duplicate samples. Each node represents a significantly enriched gene set; positively enriched sets in the FP CMs are shown in red, negatively enriched sets in the FP CMs are in blue. Node size is proportional to the total number of genes in each set, and edge thickness represents the number of overlapping genes between sets. Groups of functionally related gene sets are circled and labeled. Data represent the mean ± SEM of at least three experiments. $*p < 0.05$, $**p < 0.01$, and $***p < 0.001$. See also Figures S3 and S4.

phenotype, with fewer striations per cell but no significant reduction in the frequency of calcium transients or beat rate irregularity (Figures 3B–3E). Similarly, levels of intracellular lipid and the extent of lipid peroxidation were not increased in SP CMs over standard CMs (Figures 3F, 3G, and S3B). This suggests that SP CMs had a milder loss of sarcomeric integrity, without progression to overt lipid-induced toxicity. Upon exposure to DM, both SP and FP CMs further reduced CM score (Figure S3C), increased BNP release (Figure S3D), and increased the accumulation of intracellular lipid and lipid peroxidation (Figures S3E and S3F).

Taken together, these data indicate that a diabetic phenotype can be recapitulated in MM in FP CMs. In concordance with the milder disease phenotype of the patient of origin, SP CMs show only partial dysfunction in the absence of diabetic stress. The observation that patient-specific cells display a basal DCM phenotype that corresponds to the clinical status of the original donor is revealing. To gain a deeper understanding of the molecular changes that may underlie the differences between SP and FP cells, we compared gene-expression profiles between the two cell types using RNA sequencing. An enrichment map of the results (Figure 3H) showed that,

similar to standard CMs exposed to DM (Figure S2E), expression of genes related to DNA synthesis and mitosis was lower in the FP CMs. Furthermore, genes involved in muscle contraction and the TCA cycle were negatively enriched in the FP cells. Positively enriched genes included the glucocorticoid receptor and calcineurin-nuclear factor of activated T cells (NFAT)-signaling pathways. This result is intriguing, given that cortisol (a glucocorticoid receptor agonist) is a component of DM and that the calcium-calcineurin-NFAT pathway has well-described roles in ET-1-dependent hypertrophic CM remodeling (Drawnel et al., 2013).

High-Content Phenotypic Screening Identifies Small Molecules that Can Prevent Development of DCM In Vitro

Having established environmental and patient-specific models of DCM with linked phenotypes, we developed a screening assay to identify potential protective drugs. We conducted our primary screen on DM-treated cells, taking advantage of this rapid model. To this end, we quantified several screenable endpoints, CM score, nuclear area, and BNP production, in DM-treated cells exposed to a library of small molecules with annotated mechanisms of action (Figure 4A). To establish the minimal stimulus necessary to mimic DCM in our system, thus
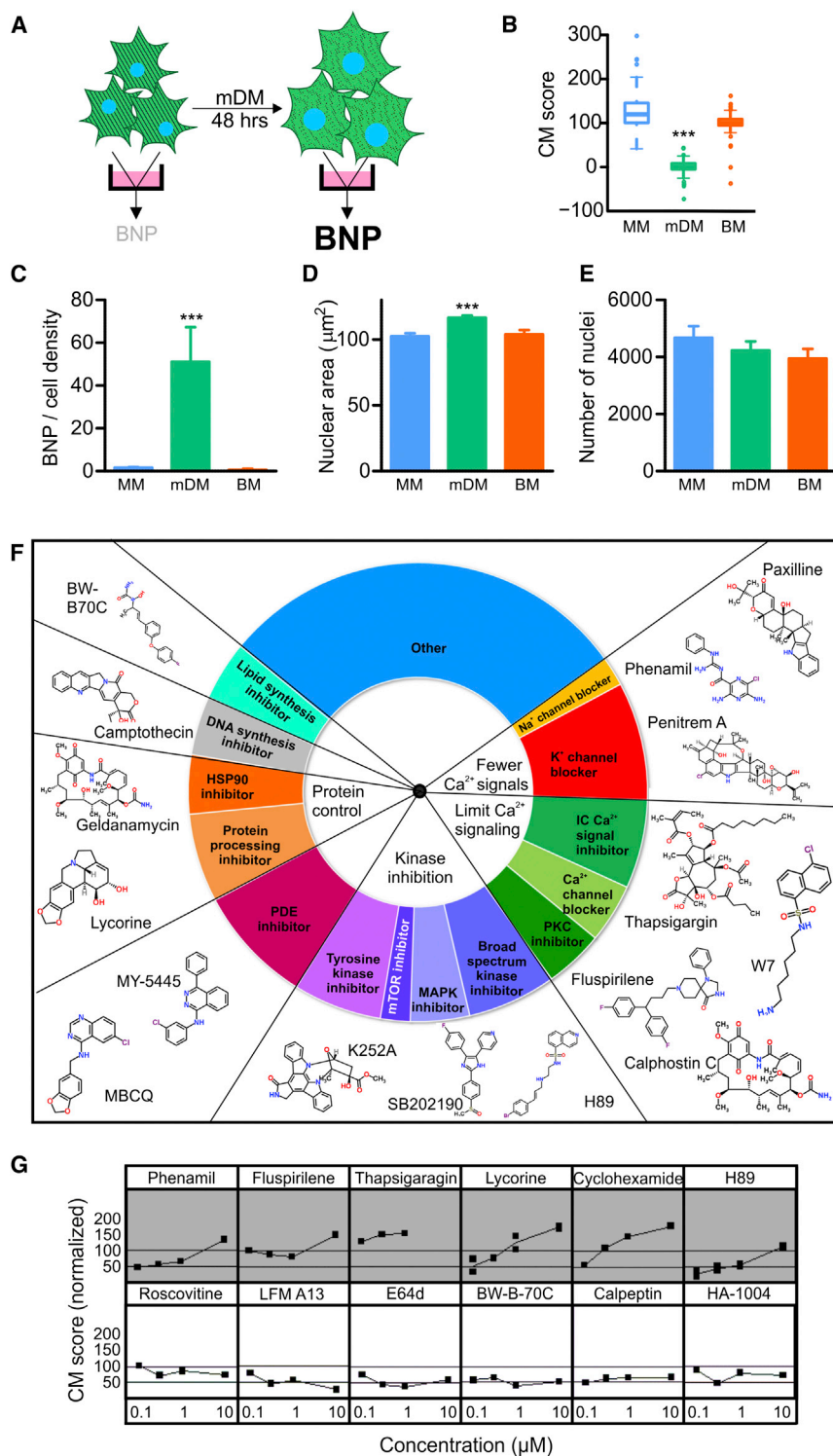
Figure 4. Phenotypic Screening for Small Molecules that Prevent Development of the DCM Phenotype

(A) Cartoon to represent the assay to measure BNP production, CM score, and nuclear area.

(B) CM score of CMs exposed to MM/mDM/BM for 2 days. BM, DM + mifepristone (10 μM) and bosentan (100 μM).

(C) BNP secretion into the culture supernatant of CMs treated as in (B).

(D) Nuclear area from IF images of CMs treated as in (B).

(E) Measurement of the number of DAPI+ nuclei per imaged region of CMs treated as in (B).

(F) Pie chart to show the functional categories of positive compounds identified in the primary screen. Compounds were categorized according to their primary mode of action, and examples of the chemical structure of selected molecules from each category are shown.

(G) Positive compounds from the primary screen were tested at 0.1, 0.3, 1, and 10 μM and CM score quantified. Six representative compounds with dose-dependent effects on CM score and six representative compounds with non-dose-dependent effects on CM score are shown. Measurements were performed in duplicate.

Data represent the mean ± SEM of at least three experiments. ***p < 0.001. See also Figures S5 and S6.

nuclear area increased (Figure 4D); and peroxidized lipid accumulated (Figures S4A and S4B). There was no change in cell number (Figure 4E). Subsequently, mDM was our negative control for assessing drug effectiveness for the prevention of dysfunction. To establish a positive control, we preincubated CMs with mifepristone to inhibit the glucocorticoid receptor and bosentan to inhibit both ET_A and ET_B receptors. A combination of 10 μM mifepristone and 100 μM bosentan (BM) effectively prevented onset of the diabetic phenotype (Figures 4B–4E). To determine assay robustness, we analyzed the effect of mDM and BM over multiple plates and experimental runs and saw consistent responses (Figures S4C and S4D). DM-treated CMs were exposed to a library of 480 compounds and CM score, nuclear area, and BNP secretion quantified after 2 days of treatment. From the initial screen, we used p value distribution analysis (Prummer, 2012) and identified 47 compounds that increase CM score, while decreasing BNP secretion and nuclear area (Figures S4E and S4F). Many of the positive compounds targeted proteins involved in calcium homeostasis (Figure 4F), including inhibitors of voltage-gated calcium channels (e.g., fluspirilene), molecules

increasing the window for drug-induced protective effects, we reduced the concentration of the three cellular stressors. We observed a similar pattern of phenotypes using the modified DM (mDM) to that produced with the original conditions: CM score declined (Figure 4B); BNP secretion increased (Figure 4C);

that deplete intracellular calcium stores (e.g., thapsigargin), and inhibitors of calcium-regulated proteins such as calmodulin (e.g., W7). We also identified sodium and potassium channel blockers (e.g., phenamil and penitrem A), which reduce the frequency of CM calcium transients. Other chemical classes were multikinase inhibitors (e.g., H89 and K252a), PDE5 inhibitors (e.g., MY-5445 and MCBQ), and protein synthesis inhibitors (e.g., lycorine and cyclohexamide). Next, to confirm efficacy and dose-dependency of response, we tested a panel of the primary hits in a dose-response assay. Twenty-eight compounds produced dose-dependent improvements in the disease parameters. Examples for CM score are shown in (Figure 4G). Trends for BNP production and nuclear area were similar (Figures S5A and S5B).

As shown in Figures S2B and S2D, DM treatment induces accumulation of intracellular peroxidized lipid and in iPSC-CMs, two of the hallmarks of DCM. We selected a variety of the confirmed hits from the screen and tested whether these molecules also prevented mDM-dependent lipid effects. BM (bosentan and mifepristone), fluspirilene, lycorine, and H89 prevented mDM-induced lipid accumulation (Figure S5C) and lipid peroxidation (Figure S5D), relative to the drugs alone. Thapsigargin was without effect on lipid accumulation or lipid peroxidation (Figures S5C and S5D). Next, we tested whether drug-induced preservation of CM structure translated into rescue of DM-induced functional deterioration by quantifying the frequency of cellular calcium transients. Similarly to DM, mDM reduced calcium transient frequency. As expected from their involvement in intracellular calcium-handling mechanisms, thapsigargin and fluspirilene dramatically reduced the basal frequency of calcium transients (Figure S5F). BM, lycorine, and H89 prevented the mDM-induced reduction in calcium transient frequency (Figures S5E and S5F).

Compounds Selected by a High-Content Phenotypic Screen Can Rescue the Phenotype of Patient-Specific CMs

Thus far, we have identified compounds that can prevent dysfunction in human CMs on exposure to the diabetic milieu, an environmental inducer of DCM. However, are these compounds able to improve the phenotype of patient-derived CMs, which is induced without environmental manipulation? To begin, we examined whether the positive control from our screening assay (BM) could rescue the basal DCM phenotype. Intriguingly, BM treatment increased CM score in both the SP and FP CMs (Figure 5A), suggesting that signaling pathways engaged by the ET and glucocorticoid receptors may be relevant to the cellular pathology in these cells. Encouraged by the efficacy of our positive control, we tested a subset of the small molecules identified in our primary screen (Figure 5B). This subset included thapsigargin, fluspirilene, H89, and lycorine, the effects of which were extensively characterized above. For the SP CMs, 14 of the 18 compounds increased CM score beyond the baseline for standard CMs (Figure 5C). In agreement with their more-severe pathology, fewer compounds were efficacious in the FP CMs (Figure 5D). Ten of the 18 compounds improved FP CM score beyond the standard cell baseline. For both cell types, the most-effective compounds were thapsigargin and fluspirilene.

DISCUSSION

Cardiovascular complications of T2DM are unfortunately a common and life-threatening occurrence. No specific drug treatment exists to prevent diabetes-induced cardiac dysfunction, a complex multifactorial condition that is distinguished by a unique set of metabolic, structural, and molecular changes within the diabetic CM. Here, we developed an in vitro screening platform for DCM, considering diabetic clinical chemistry and patient-specific cell lines. By mimicking the diabetic extracellular milieu, we created a surrogate phenotype of DCM. Suppression of this phenotype was used as a screenable endpoint to identify small molecules that prevent the development of cellular dysfunction. Furthermore, we employed diabetic patient iPSCs and showed not only a more-severe basal phenotype for patient-derived CMs but also an ability to intervene and improve the phenotype pharmacologically.

The use of glucose, ET-1, and cortisol as a prodiabetic stimulus in this study is based on findings from diabetic patients (Reynolds et al., 2010; Schneider et al., 2002). Exposure of standard cells to DM following a period of glucose restriction induced distortion of cellular structure, lipid accumulation, oxidative stress, and hypertrophy—pathological hallmarks of diabetic CMs. The same phenotype was later recapitulated in the patient-derived CMs. In our primary screen, we identified compounds that prevent induction of this phenotype and rescue the associated functional consequences. Many of these substances have been mechanisms of action compatible with what is known about the pathogenesis of diabetic cardiac dysfunction. For example, molecules that prevent calcium entry (fluspirilene and loperamide), reduce calcium in the SR (thapsigargin), or inhibit calcium-regulated proteins (W7 and CAPE) would limit the well-described pathological consequences of elevated cytosolic calcium concentration. Furthermore, gene-expression analysis revealed that the calcium-dependent calcineurin-NFAT pathway is overrepresented in the FP-CMs. Altogether, these data imply that deranged calcium cycling and signaling contributes to DCM. Interestingly, several of these molecules have been proposed as protective molecules in other iPSC models of genetic cardiomyopathies (Moretti et al., 2013). However, we also identified molecules with alternative mechanisms of action. The protein synthesis inhibitors cyclohexamide and lycorine were both identified in our primary screen, and our analysis revealed that expression of genes involved in translation and the unfolded protein response was changed in DM-treated cells. Initially, the observation that inhibition of protein synthesis can improve CM structure and function is counterintuitive, as one would predict that inhibiting synthesis of new protein would have a compounding negative effect. However, as we observed in both DM-treated CMs and the patient-specific cells, diabetic CMs experience lipotoxicity and lipid peroxidation. Both of these features are associated with the activation of proteolytic enzymes, promotion of ER stress, and leak of calcium from the SR (Ron and Walter, 2007). During ER stress, the unfolded protein response increases cellular resilience. Our expression data showed that the expression of some members of this pathway is lacking following exposure to DM. We postulate that using inhibitors of protein synthesis prevents accumulation of nascent
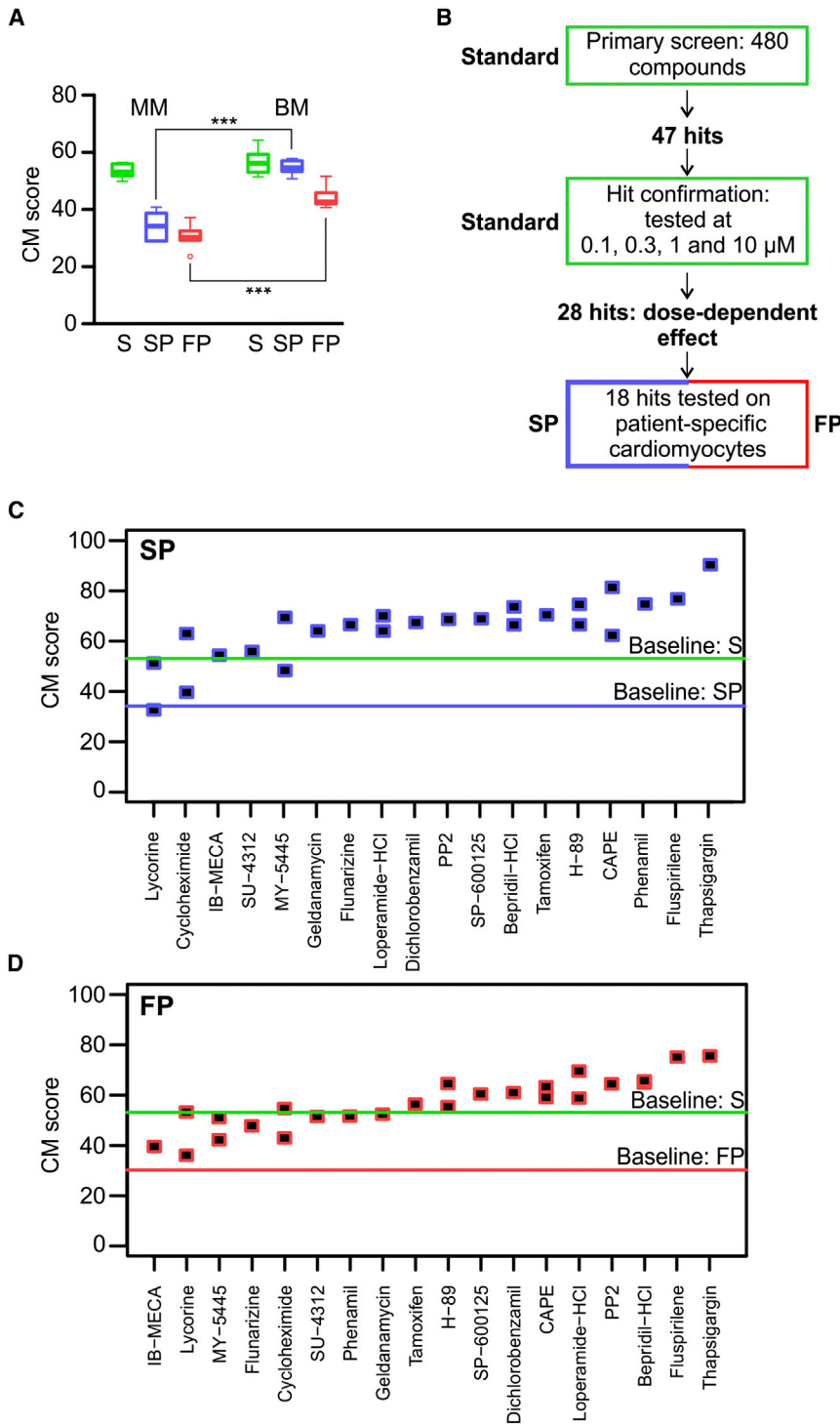
A

B

Standard → Primary screen: 480 compounds

↓ **47 hits**

Standard → Hit confirmation: tested at 0.1, 0.3, 1 and 10 μM

↓ **28 hits: dose-dependent effect**

SP ← 18 hits tested on patient-specific cardiomyocytes → **FP**

Figure 5. The Phenotype of Patient-Specific Diabetic CMs Can Be Rescued Pharmacologically

(A) CM score of S, SP, and FP CMs cultured in MM or BM for 2 days.

(B) The screening workflow from the primary screen using standard cells to testing of positive compounds on patient-specific cells.

(C) Ranked CM score in SP CMs exposed to 18 confirmed positive compounds. Compounds were tested in duplicate at 10 μM. Blue line indicates baseline CM score for the SP cells, and the green line indicates the baseline CM score for the S cells.

(D) Ranked CM score in FP CMs exposed to 18 confirmed positive compounds. Compounds were tested in duplicate at 10 μM. Red line indicates baseline CM score for the FP cells, and the green line indicates the baseline CM score for the S cells. ***p < 0.001.

C

D

tested our list of molecules on patient-specific CMs. Previous patient-specific iPSC-derived CM models have focused on well-described single-gene cardiac disorders (Moretti et al., 2013) or inherited cardiomyopathies (Lan et al., 2013; Sun et al., 2012). This reported iPSC-derived model of a complex, polygenic cardiomyopathy shows the graded phenotype of fast versus slow progression. These results raise the possibility that patient-specific models of complex disease could be used to define disease subtypes, allowing tailored drug treatments to be directed to the group of patients most suitable for their use. To definitively establish this concept, it will be necessary to derive and study CMs from a diverse set of T2DM patients.

Intriguingly, the diabetic phenotype emerges in the patient-specific cells in the absence of a diabetic stimulus, suggesting the cells are genetically/epigenetically predisposed for dysfunction. Genome-wide association studies show that multiple loci contribute to type 2 DM complications, influencing individual disease risk (Bowden, 2002). An additional layer of influence is provided by epigenetics. Exposure of cells to periods of hyperglycemia can modify the epigenome, with changes in DNA methylation

unfolded proteins and reduces load on the ER. This protects the cell from further loss of sarcomeric integrity.

In vivo testing of the predictive power of our screening assay remains an important future goal. However, such studies require investment of time and resources, which render them impractical for rapidly testing large numbers of compounds. Instead, we

persistently altering gene expression and cellular responsiveness (Siebel et al., 2010). Moreover, epigenetic-dependent "metabolic memory" has been postulated to play a role in the pathogenesis and progression of diabetic complications (Kato and Natarajan, 2014). As iPSCs can retain a memory of their prior differentiated state (Kim et al., 2011), it is plausible that CMs

differentiated from diabetic iPSCs may display a propensity toward a diabetic phenotype upon differentiation, as a consequence of epigenetically modified gene-expression patterns. In agreement with a genetic/epigenetic hypothesis, we demonstrated that the FP diabetic CMs displayed a more-extreme phenotype than the SP cells, with a heightened predisposition for dysfunction. The FP CMs were also more resistant to drug treatment. These observations are consistent with the faster clinical progression of the FP patient and suggest that the FP patient may carry a more-severe combination of polymorphisms/modifications. Interestingly, neither FP nor SP CMs released more BNP basally than standard CMs (Figure S3D), although all cell types released BNP in response to DM. These data are in concordance with the retention of structural disruption but fall in BNP release observed in standard cells after DM removal (Figures S1F–S1H), suggesting that continued external cellular stress is required to induce BNP production. In contrast, structural disarray appears to be maintained by persistent genetic/epigenetic alterations to intracellular pathways. Further studies should address comparison of the genome and epigenome of the cells utilized here, in order to establish the origin of the predisposition for cellular pathology.

In conclusion, we have established a paradigm in the search for effective treatments for DCM. We show that, by using iPSC-derived CMs, a disease with complex and multifactorial etiology can be modeled in vitro and strategies for drug treatment tested on different patient groups. This powerful platform has the potential to discover new disease mechanisms and target treatments to the most-appropriate individuals, enhancing both specificity and efficacy.

EXPERIMENTAL PROCEDURES

Detailed descriptions of the experimental procedures are given in the Supplemental Information.

CM Culture
CMs derived from CDI-MRB iPSCs (Cellular Dynamics International [CDI]) were thawed at 37°C for 3 min and resuspended in plating medium (CDI). We plated 35,000 viable cells per well on fibronectin-coated (Sigma) BD falcon 96-well imaging plates and rested at room temperature for 30 min. Cells were incubated at 37°C, 7% CO$_2$ for 48 hr, and then plating medium was exchanged for maturation medium (MM) for 72 hr. MM is Dulbecco's modified Eagle's medium no glucose (GIBCO), 10 mM HEPES, 2 mM L-carnitine, 5 mM creatine, 5 mM taurine, 1 mM nonessential amino acids (GIBCO), 1× insulin-transferrin-selenium (Sigma-Aldrich), and linoleic-oleic acid (Sigma-Aldrich). After 72 hr, MM was exchanged for DM (MM plus 10 mM glucose, 10 nM h-endothelin-1, and 1 μM cortisol) or MM + vehicle control for a further 2 days.

Patient-Derived CMs
Human iPSC lines were derived from anonymized human skin biopsies following full informed consent and approval by the Partners Healthcare Human Research Committee (protocol number 2010-P-000122/1). iPSCs were generated by retroviral reprogramming using OCT4, SOX2, KLF4, and c-MYC and checked for pluripotency and normality of karyotype. iPSC lines were transferred to CDI for differentiation into cardiomyocytes. Following cardiomyocyte production, culture protocols were identical to those used for the standard cardiomyocytes.

Imaging and Analysis
Imaging was performed using the PerkinElmer Operetta imaging system with a 20× objective. Per well, nine fields of view were captured and DAPI-stained nuclei identified with Harmony software. More than 2,500 cells were analyzed per condition. Nuclear area was determined using the DAPI signal. To quantify intracellular lipid/peroxidation, the intensity of fluorescence in the cell region was measured. For the determination of CM score, a custom algorithm implemented in the PerkinElmer image analysis software Acapella was developed. Briefly, extended striation patterns were quantified using a pair of nonlinear texture filters to enhance linear bright and dark features and subsequent cross-correlation. From extracted features, such as the modulation amplitude of the correlation image, a "CM score" was constructed as the proportion of striated cells in the sample. For full details, see the Supplemental Information.

Statistical Analysis
Unless otherwise stated, all experiments were minimally performed in triplicate. Results are presented as mean ± SEM. Statistical analyses were performed in GraphPad Prism using the one-sample t test for two groups and one-way ANOVA followed by Tukey analysis for two or more groups. $p < 0.05$ was considered significant. Statistical analysis of the small molecule screen is described in the Supplemental Experimental Procedures.

ACCESSION NUMBERS

The microarray data reported in this paper have been deposited to the NCBI Gene Expression Omnibus and are available under accession number GSE62203.

SUPPLEMENTAL INFORMATION

Supplemental Information includes Supplemental Experimental Procedures, five figures, and three tables and can be found with this article online at http://dx.doi.org/10.1016/j.celrep.2014.09.055.

AUTHOR CONTRIBUTIONS

F.M.D., S.B., F.D., A.G., N.A., M.P., J.-C.H., A.K., L. Badi, T.K.-T., R.G., M.W., E.J., L. Bu, X.J., and J.B. performed/analyzed experiments, and F.M.D., S.B., J.B., B.J.H., K.R.C., K.K., M. Burcin, M. Boehringer, C.C., G.G., M.C.M., H.S., and R.I. designed experiments. F.M.D. and R.I. interpreted the data. F.M.D., K.K., M.P., and R.I. wrote the manuscript.

REFERENCES

Abassi, Y.A., Xi, B., Li, N., Ouyang, W., Seiler, A., Watzele, M., Kettenhofen, R., Bohlen, H., Ehlich, A., Kolossov, E., et al. (2012). Dynamic monitoring of beating periodicity of stem cell-derived cardiomyocytes as a predictive tool for preclinical safety assessment. Br. J. Pharmacol. *165*, 1424–1441.

Bers, D.M. (2008). Calcium cycling and signaling in cardiac myocytes. Annu. Rev. Physiol. *70*, 23–49.

Bowden, D.W. (2002). Genetics of diabetes complications. Curr. Diab. Rep. *2*, 191–200.

Carlson, C., Koonce, C., Aoyama, N., Einhorn, S., Fiene, S., Thompson, A., Swanson, B., Anson, B., and Kattman, S. (2013). Phenotypic screening with human iPS cell-derived cardiomyocytes: HTS-compatible assays for interrogating cardiac hypertrophy. J. Biomol. Screen. *18*, 1203–1211.

Devereux, R.B., Roman, M.J., Paranicas, M., O'Grady, M.J., Lee, E.T., Welty, T.K., Fabsitz, R.R., Robbins, D., Rhoades, E.R., and Howard, B.V. (2000). Impact of diabetes on cardiac structure and function: the strong heart study. Circulation *101*, 2271–2276.

Drawnel, F.M., Archer, C.R., and Roderick, H.L. (2013). The role of the para-crine/autocrine mediator endothelin-1 in regulation of cardiac contractility and growth. Br. J. Pharmacol. *168*, 296–317.

Heather, L.C., and Clarke, K. (2011). Metabolism, hypoxia and the diabetic heart. J. Mol. Cell. Cardiol. *50*, 598–605.

Kato, M., and Natarajan, R. (2014). Diabetic nephropathy—emerging epige-netic mechanisms. Nat. Rev. Nephrol. *10*, 517–530.

Kim, K., Zhao, R., Doi, A., Ng, K., Unternaehrer, J., Cahan, P., Huo, H., Loh, Y.-H., Aryee, M.J., Lensch, M.W., et al. (2011). Donor cell type can influence the epigenome and differentiation potential of human induced pluripotent stem cells. Nat. Biotechnol. *29*, 1117–1119.

Lan, F., Lee, A.S., Liang, P., Sanchez-Freire, V., Nguyen, P.K., Wang, L., Han, L., Yen, M., Wang, Y., Sun, N., et al. (2013). Abnormal calcium handling properties underlie familial hypertrophic cardiomyopathy pathology in pa-tient-specific induced pluripotent stem cells. Cell Stem Cell *12*, 101–113.

Lopaschuk, G.D., and Jaswal, J.S. (2010). Energy metabolic phenotype of the cardiomyocyte during development, differentiation, and postnatal maturation. J. Cardiovasc. Pharmacol. *56*, 130–140.

Lorenzo, O., Ramírez, E., Picatoste, B., Egido, J., and Tuñón, J. (2013). Alteration of energy substrates and ROS production in diabetic cardiomyopa-thy. Mediators Inflamm. *2013*, 461967.

Ma, J., Guo, L., Fiene, S.J., Anson, B.D., Thomson, J.A., Kamp, T.J., Kolaja, K.L., Swanson, B.J., and January, C.T. (2011). High purity human-induced pluripotent stem cell-derived cardiomyocytes: electrophysiological properties of action potentials and ionic currents. Am. J. Physiol. Heart Circ. Physiol. *301*, H2006–H2017.

Mandavia, C.H., Aroor, A.R., Demarco, V.G., and Sowers, J.R. (2013). Molecular and metabolic mechanisms of cardiac dysfunction in diabetes. Life Sci. *92*, 601–608.

Minamino, T., and Kitakaze, M. (2010). ER stress in cardiovascular disease. J. Mol. Cell. Cardiol. *48*, 1105–1110.

Moretti, A., Laugwitz, K.L., Dorn, T., Sinnecker, D., and Mummery, C. (2013). Pluripotent stem cell models of human heart disease. Cold Spring Harb Perspect Med *3*. http://dx.doi.org/10.1101/cshperspect.a014027.

Prummer, M. (2012). Hypothesis testing in high-throughput screening for drug discovery. J. Biomol. Screen. *17*, 519–529.

Reynolds, R.M., Labad, J., Strachan, M.W.J., Braun, A., Fowkes, F.G.R., Lee, A.J., Frier, B.M., Seckl, J.R., Walker, B.R., and Price, J.F.; Edinburgh Type 2 Diabetes Study (ET2DS) Investigators (2010). Elevated fasting plasma cortisol is associated with ischemic heart disease and its risk factors in people with type 2 diabetes: the Edinburgh type 2 diabetes study. J. Clin. Endocrinol. Metab. *95*, 1602–1608.

Ron, D., and Walter, P. (2007). Signal integration in the endoplasmic reticulum unfolded protein response. Nat. Rev. Mol. Cell Biol. *8*, 519–529.

Schneider, J.G., Tilly, N., Hierl, T., Sommer, U., Hamann, A., Dugi, K., Leidig-Bruckner, G., and Kasperk, C. (2002). Elevated plasma endothelin-1 levels in diabetes mellitus. Am. J. Hypertens. *15*, 967–972.

Siebel, A.L., Fernandez, A.Z., and El-Osta, A. (2010). Glycemic memory associated epigenetic changes. Biochem. Pharmacol. *80*, 1853–1859.

Steinberg, S.F. (2013). Oxidative stress and sarcomeric proteins. Circ. Res. *112*, 393–405.

Sun, N., Yazawa, M., Liu, J., Han, L., Sanchez-Freire, V., Abilez, O.J., Navar-rete, E.G., Hu, S., Wang, L., Lee, A., et al. (2012). Patient-specific induced pluripotent stem cells as a model for familial dilated cardiomyopathy. Sci. Transl. Med. *4*, 30ra47.

Taegtmeyer, H., Sen, S., and Vela, D. (2010). Return to the fetal gene program: a suggested metabolic link to gene expression in the heart. Ann. N Y Acad. Sci. *1188*, 191–198.

Yang, X., Pabon, L., and Murry, C.E. (2014). Engineering adolescence: maturation of human pluripotent stem cell-derived cardiomyocytes. Circ. Res. *114*, 511–523.